

Article

Simple and Intelligent Electrochemical Detection of Ammonia over Cuprous Oxide Thin Film Electrode

Samia A. Kosa ¹, Amna N. Khan ¹, Basma Al-Johani ¹, L. A. Taib ¹, M. Aslam ², Wafa A. Bawazir ¹,
A. Hameed ^{2,3} and M. Tahir Soomro ^{2,*}

¹ Department of Chemistry, Faculty of Science, King Abdulaziz University, Jeddah 21589, Saudi Arabia; skousah@kau.edu.sa (S.A.K.); ank mohamad@kau.edu.sa (A.N.K.); mencomwelicom@hotmail.com (B.A.-J.); ltaib@kau.edu.sa (L.A.T.); wbawazeer@kau.edu.sa (W.A.B.)

² Centre of Excellence in Environmental Studies (CEES), King Abdulaziz University, Jeddah 21589, Saudi Arabia; mainayatullah@kau.edu.sa (M.A.); ahfmuhammad@gmail.com (A.H.)

³ National Center of Physics, Quaid-e-Azam University, Islamabad 44000, Pakistan

* Correspondence: soomro.m.tahir@gmail.com or mssoomro@kau.edu.sa

Abstract: To realize simple and intelligent electrochemical ammonia (NH₃) detection in water, highly dense colloidal copper nanoparticles (CuNPs) were prepared and subsequently deposited onto a glassy carbon electrode (GCE). The CuNPs/GCE was then placed in an oven at 60 °C to intelligently transform CuNPs into cuprous oxide (Cu₂O) thin film. The colloidal CuNPs were characterized by ultraviolet-visible (UV-Vis) spectroscopy, whereas the fabricated Cu₂O/GCE was subjected to Fourier transform infrared spectroscopy (FTIR), X-ray diffraction (XRD), X-ray photoelectron spectroscopy (XPS), scanning electron microscopy (SEM), and electrochemical impedance spectroscopy (EIS). The XRD of Cu₂O/GCE showed the crystalline nature of the thermally converted Cu₂O thin film, whereas XPS demonstrated that the thin film formed on the surface of GCE was primarily composed of Cu₂O. The SEM images of Cu₂O/GCE revealed Cu₂O crystals with hexapod morphology. The EIS study exhibited substantially higher charge transfer activity of Cu₂O/GCE compared to bare GCE. The drop coating of ammonia (NH₃) solution onto Cu₂O/GCE enabled the fabricated electrode to be utilized as an electrochemical sensor for NH₃ detection in water. The cyclic voltammetric (CV) behavior of NH₃/Cu₂O/GCE was investigated in 0.1 M pH 7 phosphate buffer, which led to the formation of a copper-ammonia complex and revealed the nobility of the fabricated electrode. The square wave voltammetric (SWV) response was linear over the 10 μM and 1000 μM ranges with a detection limit of 6.23 μM and good reproducibility. The NH₃/Cu₂O/GCE displayed high selectivity for the detection of NH₃ in the presence of various coexisting cations and anions in 0.1 M pH 7 phosphate buffer. The recovery of NH₃ in the drinking water sample varied from 98.2% to 99.1%.

Keywords: cuprous oxide; thin film; ammonia; complex; electrochemical detection



Citation: Kosa, S.A.; Khan, A.N.; Al-Johani, B.; Taib, L.A.; Aslam, M.; Bawazir, W.A.; Hameed, A.; Soomro, M.T. Simple and Intelligent Electrochemical Detection of Ammonia over Cuprous Oxide Thin Film Electrode. *Surfaces* **2023**, *6*, 430–449. <https://doi.org/10.3390/surfaces6040029>

Academic Editor: Gaetano Granozzi

Received: 1 September 2023

Revised: 6 October 2023

Accepted: 20 October 2023

Published: 6 November 2023



Copyright: © 2023 by the authors. Licensee MDPI, Basel, Switzerland. This article is an open access article distributed under the terms and conditions of the Creative Commons Attribution (CC BY) license (<https://creativecommons.org/licenses/by/4.0/>).

1. Introduction

The determination of ammonia in water is particularly important because of its toxic and irritant effects [1,2]. And, because of the widespread use of ammonia in food processing, agriculture, cleaning and disinfectant products, and refrigeration, excess ammonia can significantly harm the environment and human health [3]. The detection of ammonia in water has been reported through colorimetric/spectroscopic methods, however, time consumption, labor requirements, and associated high costs often limit their regular use [4–6]. Several researchers have also reported the amperometric/potentiometric detection of ammonia [7–12]. However, from the viewpoint of wastewater treatment, application in the ammonia fuel cell, and as a source for ultra-pure hydrogen, most of the detection of ammonia has been focused on its electrochemical oxidation in alkaline solution [13–16]. Based on the fabricated electrode system, a few methods have also been developed to detect the presence of ammonia in water, however, the lack of simplicity in fabrication

is a significant shortcoming [3,17]. In this regard, the synthesis of colloidal CuNPs, their fabrication as Cu₂O thin film on GCE, and drop coating of NH₃ solution onto Cu₂O/GCE for the detection of NH₃ through copper-ammonia complex formation is a novel and simple approach to report.

CuNPs are striking materials primarily due to their intrinsic properties and wide range of applications in various fields, including photocatalysis, perovskite solar cells, energy conversion, electrochemical detection/sensing, biosensing, gas sensors, and antimicrobial activity [18–20]. Due to their high electrical conductivity and chemical reactivity, CuNPs are also replacing Au and Ag in conductive pastes and catalysis applications [21,22]. Recently, CuNPs have been of particular interest in electrochemical detection applications as well. As a result, CuNP-based electrodes have emerged in the past few years as the most suitable alternative for the direct monitoring of a variety of analytes [23–25]. Due to copper-ammonia complex affinity [26,27], CuNPs can be an efficient electrode material for the simple electrochemical detection of NH₃. However, the only report appears to be from Valentini et al. [17], who used multi-walled carbon nanotube/copper nanoparticles composite paste electrodes for the detection of NH₃ in drinking water. The disadvantages of this method include the complicated fabrication steps, vague mechanism, and poor reproducibility of the proposed electrode.

Among the various chemical methods for the synthesis of CuNPs, the wet chemical reduction method offers several advantages over others [28–30]. It is economical, simple, requires less effort, provides better control over the particle size and distribution, and flexibility in terms of the dense packing of CuNPs as thin films. However, the stability of colloidal CuNPs is extremely critical due to their sensitivity to air and the permanence of their oxides [31,32]. In recent years, reducing agents with additional capping and binding properties have received much attention due to their capability of modifying the NP surfaces in such a way as to increase their loading on substrates and produce functional thin films [28,33–35]. One such reducing agent is ascorbic acid, which is known to functionalize CuNPs while reducing them to a stable colloidal form.

There has been much interest in electrochemical sensing applications of Cu₂O NPs due to their narrow band gap and excellent electrical properties [36]. As a result, various synthesis routes have been employed to obtain Cu₂O NP-fabricated GCE. One such unique route consisted of oxidizing colloidal CuNPs on the surface of GCE at a low temperature (<250 °C) in the air [37,38]; however, to the best of our knowledge, this strategy was not employed in electrochemical sensing applications of Cu₂O NPs. On the other hand, copper-ammonia chemistry is well established in the literature regarding the electrodeposition of Cu from ammonia solution because of the diverse speciation of Cu₂O and CuO [37,38]; however, no NH₃ detection was proposed earlier. Thus, oxidizing colloidal CuNPs on the surface of GCE under controlled thermal treatment in Cu₂O is an intelligent and unique way to report the detection of NH₃.

Herein, colloidal CuNPs were prepared through a wet chemical reduction method using ascorbic acid as a reducing as well as stabilizing agent. Prepared CuNPs were subsequently deposited on GCE and oxidized into Cu₂O thin film in an oven at 60 °C. For the detection of NH₃, Cu₂O/GCE was further modified with NH₃ solution and investigated by CV in 0.1 M pH 7 phosphate buffer. Suitable reaction pathways have been proposed corresponding to the reduction of the copper-ammonia complex, which produced a new reduction peak. Based on this, an intelligent NH₃ detection in water is presented here.

2. Experimental Section

2.1. Reagents and Solutions

Copper(II) nitrate (Cu(NO₃)₂, 99%), ascorbic acid, sodium hydroxide (NaOH), phosphoric acid (H₃PO₄), ammonia (NH₃) solution (32%), potassium chloride (KCl), potassium ferricyanide (Fe(CN)₆^{3-/4-}), and sodium sulfate (Na₂SO₄) were purchased from Sigma-Aldrich and used without any further modification. Then, 0.1 M stock solution of NH₃ was prepared in deionized water. The 0.1 M phosphate buffers of various pH were prepared by

the appropriate mixing of 0.5 M H_3PO_4 and 0.5 M NaOH solutions. The working solutions of NH_3 were prepared by diluting the stock solution with phosphate buffer; 0.1 M KCl and 0.1 M NaSO_4 were also tested as supporting electrolytes.

2.2. Synthesis of Colloidal CuNPs

Highly dense colloidal CuNPs were prepared in a single pot using the wet chemical reduction method. Briefly, 1 mL of 0.3 M $\text{Cu}(\text{NO}_3)_2$ was mixed with an appropriate amount of 0.5 M ascorbic acid and 0.2% NaOH under stirring. The reaction mixture was then refluxed for 2 h at 80 °C in air until the complete reduction of the metallic salt. During the reaction, the color changed from colorless to pale yellow, orange, pale brown, and, finally, dark brown. The volume of the reaction vessel was kept constant at 10 mL during the reduction process. The purpose of adding NaOH was to accelerate the rate of reduction. Ascorbic acid served as both a reducing and stabilizing agent. The reaction mixture was cooled and kept at room temperature for further studies.

2.3. Preparation of Cu_2O Thin Film Electrode

For thin film formation, about 1 mL of the colloidal CuNPs was diluted with deionized water and sonicated for 2 min to obtain a homogeneous solution. The surface of GCE was thoroughly cleaned through polishing on alumina and diamond slurries, respectively, subsequently washed, and air dried. About 20 μL of colloidal CuNPs was dropped on GCE to cover the entire surface. The uniformity of the coated surface was optically ensured and left in an oven at 60 °C for 5 min. The drop-coated CuNPs were oxidized into a Cu_2O thin film during the drying process and labeled as $\text{Cu}_2\text{O}/\text{GCE}$.

2.4. Apparatus

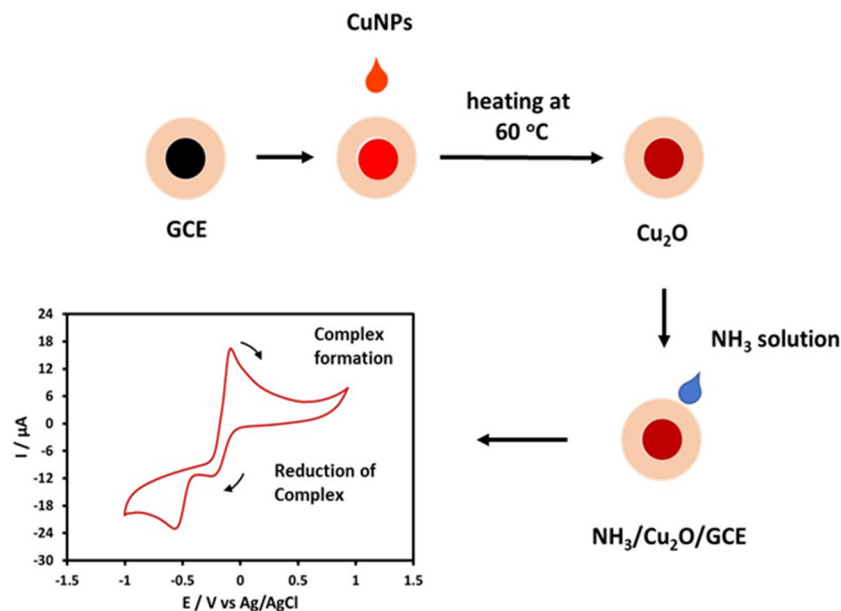
The UV-visible spectra of colloidal CuNPs were recorded on a Cary 60 (Agilent Technology, Santa Clara, CA, USA). Fourier transform infrared (FTIR) analysis of $\text{Cu}_2\text{O}/\text{GCE}$ was performed with a Cary 630 (Agilent Technology, USA). The crystallinity of thermally converted Cu_2O thin film on GCE was studied using an automated multipurpose X-ray diffractometer (Ultima IV, Rigaku, Akishima, Japan) equipped with $\text{Cu K}\alpha$ radiation source in the 2θ range of 10° to 80°, at a 40 kV accelerating voltage, and a current of 40 mA. The elemental composition was analyzed by XPS (PHI 5000 Versa Probe II, ULVAC-PHI Inc., Chigasaki, Japan) in the binding energy range of 0 eV to 1350 eV. The shape, aggregation, and distribution information of Cu_2O thin film on GCE was obtained using a field emission electron microscope (FESEM, JEOL, JSM-IT700HR, Tokyo, Japan). Electrochemical measurements including EIS, CV, and SWV were carried out with a VSP multi-channel potentiostat (Bio-logic Science Instrument, Seyssinet-Pariset, France) in a 20-mL cell with a three-electrode assembly. The assembly had a 3-mm diameter glassy carbon working electrode, a 50-mm long with a 0.5-mm diameter Pt wire counter electrode, and an Ag/AgCl reference electrode.

2.5. EIS and Electrochemical Measurements

Throughout the electrochemical measurements, the nitrogen environment was maintained. The EIS data were obtained against 2 mM $(\text{Fe}(\text{CN})_6)^{3-/4-}$ in 0.1 M KCl by scanning the frequency between 100 mHz–100 kHz at a 10 mV AC amplitude. The Nyquist plots were extracted using Randle's equivalent circuit model. CV scans were initiated at all times at open circuit voltage (OCV) to a vertex potential (E_1) +1.0 V followed by a cathodic sweep from +1.0 V to −1.0 V and an anodic sweep from −1.0 V to +1.0 V at a scan rate of 100 mV/s in 0.1 M pH 7 phosphate buffer. A series of optimizations were performed with SWV in the potential direction from +1.0 V to −1.0 V to construct the calibration curves and calculate the limit of detection. No OCV or accumulation time was employed during SWV. For the interference study, reagent-grade chemicals were used.

2.6. NH_3 Detection Procedure

An amount of 10 μL of 1 mM NH_3 was dropped onto $\text{Cu}_2\text{O}/\text{GCE}$ and dried in air before the electrochemical measurements. The as-prepared $\text{NH}_3/\text{Cu}_2\text{O}/\text{GCE}$ was then immersed in an electrochemical cell containing 0.1 M pH 7 phosphate buffer to obtain the CV behavior of NH_3 , as shown in Scheme 1. For analytical detection, $\text{NH}_3/\text{Cu}_2\text{O}/\text{GCE}$ with various concentrations of NH_3 were separately prepared using the drop coating procedure and subjected to SWV under the optimized conditions.



Scheme 1. Schematic representation of the preparation of $\text{NH}_3/\text{Cu}_2\text{O}/\text{GCE}$ and CV analysis.

2.7. NH_3 Recovery in Drinking Water

The drinking water sample was collected from Jeddah, Saudi Arabia. The sample was filtered using a 0.45- μm membrane filter to remove solid particulates and kept refrigerated at 4 $^\circ\text{C}$. The sample was diluted with 0.1 M of pH 7 phosphate buffer and the SWV response of $\text{Cu}_2\text{O}/\text{GCE}$ was recorded under the optimized conditions. For recovery, the stock solution of NH_3 was quantitatively dropped and coated onto $\text{Cu}_2\text{O}/\text{GCE}$, and the SWV scans of the various $\text{NH}_3/\text{Cu}_2\text{O}/\text{GCE}$ s were recorded in drinking water samples adjusted with 0.1 M pH 7 phosphate buffer.

3. Results and Discussion

3.1. UV-Visible Spectra of Colloidal CuNPs

Figure 1 shows the absorption spectra obtained at different times and the color change due to the formation of colloidal CuNPs. In an aqueous solution, CuNPs exhibited a broad and strong absorption signal around ~ 428 nm, corresponding to the surface plasmon resonance (SPR) of CuNPs. Ascorbic acid treatment is responsible for the broadening of CuNP SPR accompanied by a blue shift, indicating the formation and growth of smaller well-dispersed CuNPs, as reported elsewhere [28].

The increase in absorbance was due to the continuous growth of CuNPs in aqueous solution. The absorbance reached a maximum at 120 min as there was no further change in the color or UV-Vis spectra witnessed indicating that Cu salt completely reduced into CuNPs. The time required to produce CuNPs is much less than reported in the literature [28]. The additional absorption peak at ~ 330 nm was assigned to the oxidation product of ascorbic acid according to the literature [28].

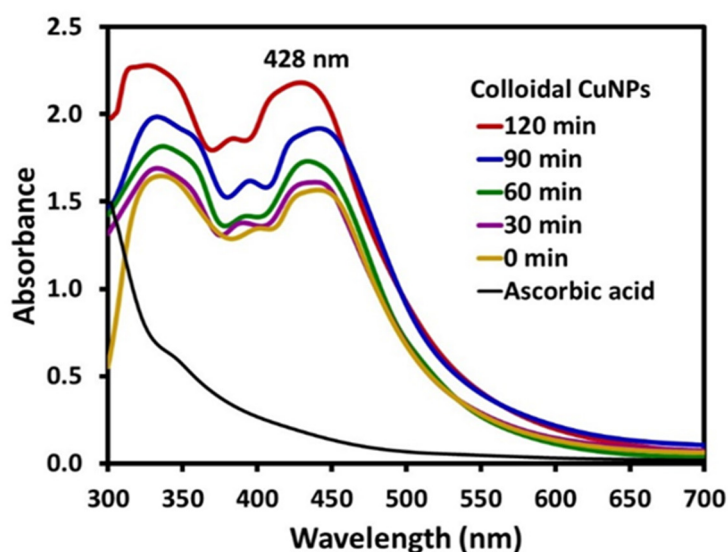


Figure 1. Absorption spectra of CuNPs at different time intervals and color transformation.

3.2. Surface Functional Group Analysis by FTIR

The provision of ascorbic acid in the Cu_2O thin film formation on GCE was studied by FTIR. The typical IR spectrum of pure ascorbic acid is presented in Figure 2, where characteristic peaks appeared at 3021 , 1775 , 1664 , 1329 , and 1108 cm^{-1} , respectively [29,39]. A group of peaks in the region $3216\text{--}3529$ were unassigned and were due to the O-H stretches. The peak at 3021 cm^{-1} was assigned to the =C-H stretching vibrations. The C=O bond stretching was observed at 1775 cm^{-1} , whereas the 1664 cm^{-1} vibrations belonged to the C=C. The stretching at 1329 cm^{-1} originated from the C-O-C functional group. The C-O-H bond probably contributed to the peak at 1108 cm^{-1} . In the IR spectrum of Cu_2O thin film (Figure 2), the peaks associated with C=O and C-O-H bonds disappeared.

Ascorbic acid fully oxidized into dehydroascorbic acid when CuNPs occurred in colloidal solution [40]. However, during Cu_2O thin film formation, as the Cu^0 reoxidized into Cu^+ , it is highly likely that dehydroascorbic acid converted into semi-dehydroascorbic acid form [41–43]. This is inferred from the IR spectrum of $\text{Cu}_2\text{O}/\text{GCE}$, as the peak correlated with C=C and C-O-C remained but shifted to a lower wavenumber due to the significant delocalization of conjugated C=C bonds. Moreover, the peak at 600 cm^{-1} can be assigned to the vibrations of the Cu-O bond [44]. Considerable differences in the IR spectra provided clear evidence of the presence and aiding of ascorbic acid in the Cu_2O thin film formation on GCE.

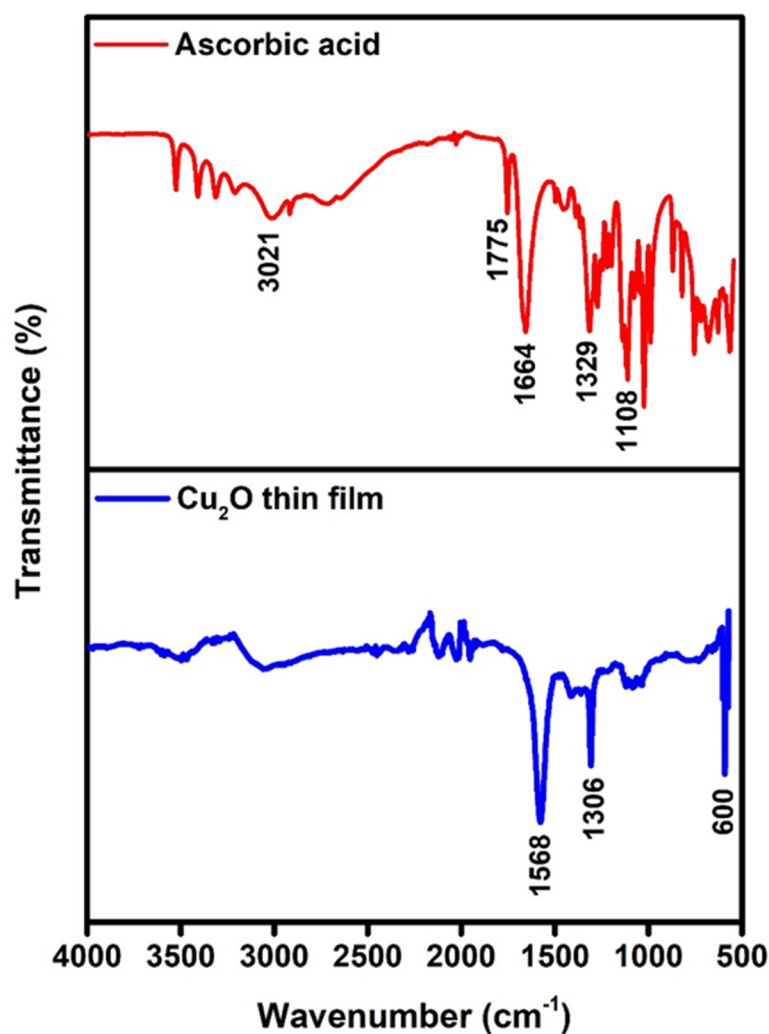


Figure 2. FTIR analysis of pure ascorbic acid and Cu₂O/GCE.

3.3. X-ray Diffraction Pattern of Cu₂O/GCE

The crystal structure of Cu₂O thin film on GCE was studied by XRD. The obtained XRD pattern of Cu₂O/GCE is presented in Figure 3, where the peaks at 30.6°, 37.4°, 42.6°, 61.4°, and 72.4° corresponded to the 110, 111, 200, 220, and 311 planes of cuprite, indicating the crystalline nature of Cu₂O thin film formed on GCE. The observed peak positions were well-matched with JCPDS# 05-0667, confirming the presence of body-centered cubic (bcc) Cu₂O on the surface of GCE as a thin film [29,45,46]. The XRD spectrum indicated that peaks indexed to Cu₂O were dominated in the spectrum, ruling out the presence of CuO in the film formed on the surface of GCE. The peaks indicated by -asterisk in the spectrum were due to the ascorbic acid adduct [47] and showed polycrystalline behavior, which is necessary and favorable in integrating Cu₂O as a thin film on the surface of GCE.

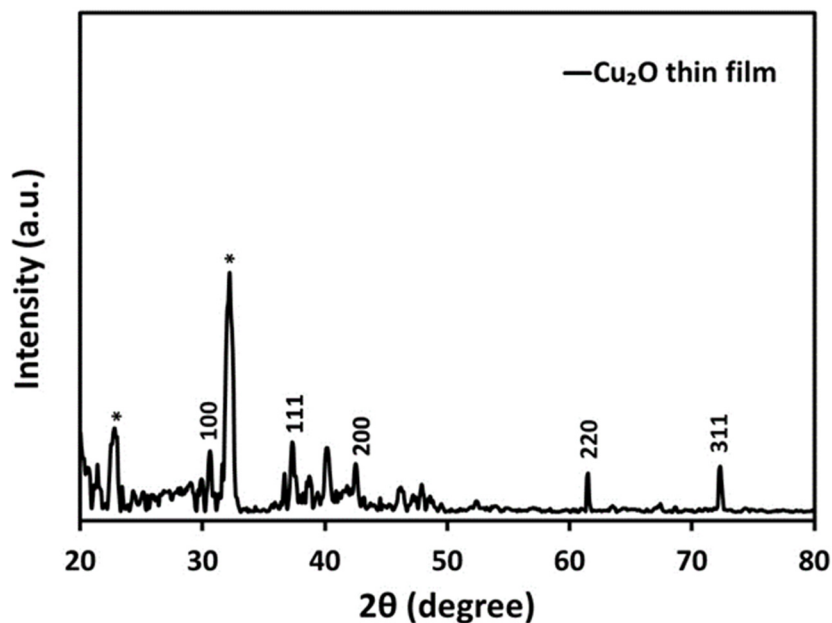


Figure 3. XRD diffraction pattern of $\text{Cu}_2\text{O}/\text{GCE}$. Asterisks mark the diffractions peaks from ascorbic acid adduct.

3.4. XPS Analysis

The structure of the Cu_2O thin film formed on GCE was further investigated by XPS. The obtained high-resolution XPS spectra are illustrated in Figure 4, where the symmetrical peak related to $\text{Cu}2p_{1/2}$ appeared at ~ 952.9 eV with no or minimal satellite formation, suggesting that the film was primarily composed of Cu_2O . The $\text{Cu}2p_{3/2}$ corresponding to Cu^+ in Cu_2O after fitting was observed at 932.8 eV [48,49]. Furthermore, the peak located at 530.15 consisted of the signature of O1s peak of Cu_2O based on literature interpretations. Thus, both XRD and XPS analysis showed no evidence of the presence of Cu^{2+} in the film.

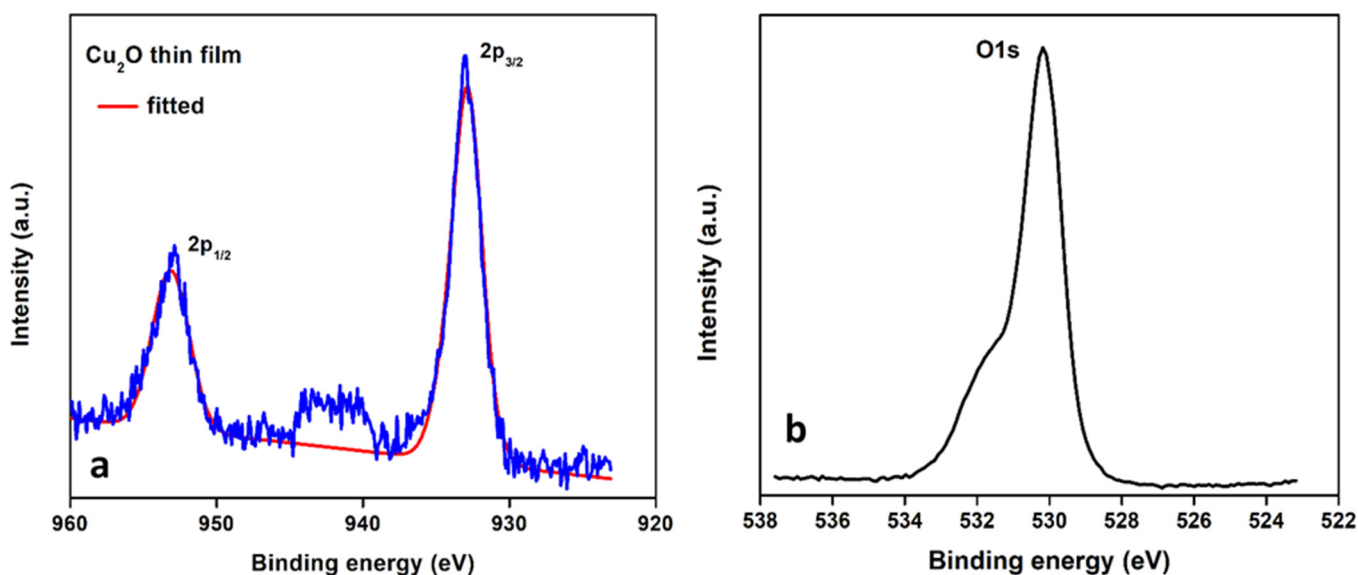


Figure 4. High-resolution XPS spectra of Cu_2O thin film (a) $\text{Cu}2p$ and (b) O1s.

3.5. Morphology of Cu_2O on GCE

The morphology of Cu_2O spread on the surface of GCE was characterized by SEM analysis. Figure 5a–d shows the SEM images of $\text{Cu}_2\text{O}/\text{GCE}$ at different magnifications,

where the presence of a micron-sized hexapod was evident on $\text{Cu}_2\text{O}/\text{GCE}$ [50–52]. For comparison, an SEM image of bare GCE is provided in Figure S1 (Supplementary Information), where no particles were observed. In Figure 5a,b, images at $1500\times$ magnification show that hexapod Cu_2O with different growth stages, i.e., long- and short-leg-sized particles, were substantially populated on the surface of GCE. CuNPs were prone to oxidation in the air. When spread on GCE as a thin film, under controlled heat treatment at 60°C , CuNPs mainly transformed into the Cu_2O phase because CuO formation was reported at an even higher temperature $>250^\circ\text{C}$ [37,38]. The controlled heat treatment also affected the size and morphology of the CuNP film and, upon reaction with oxygen, the micron-sized Cu_2O with a characteristic hexapod morphology was formed on the surface of GCE, as confirmed by XRD and XPS analysis. Thus, the thermal treatment of colloidal CuNPs spread on the surface of GCE is a novel and simple way to produce hexapod Cu_2O as a thin film. Higher magnification (Figure 5c,d) revealed that the larger hexapods appeared to be formed by an aggregation of smaller particles. Also, the smooth faces of larger hexapods were the result of the steady growth and surface reconstruction. Alongside the area coverage by the Cu_2O hexapod, which improved the current response of the modified electrode, the exposed facets of Cu_2O were also reported to play an important role in defining the electrochemical performance of the modified electrode [50]. As a result, due to the excellent conductivity of Cu_2O hexapods and their affinity towards copper-ammonia complex formation, the highly sensitive detection of NH_3 on $\text{Cu}_2\text{O}/\text{GCE}$ was expected.

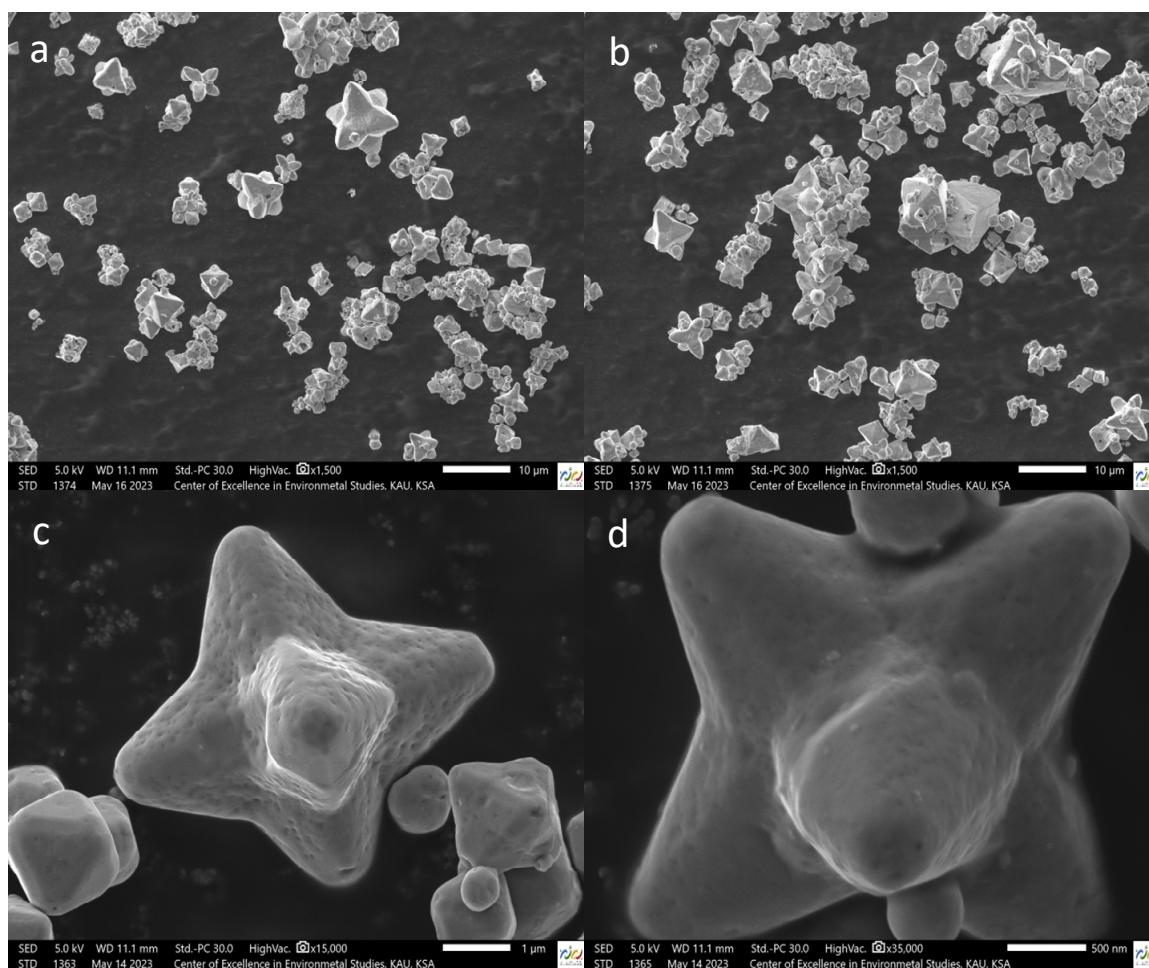


Figure 5. SEM images of $\text{Cu}_2\text{O}/\text{GCE}$ at different magnifications (a,b) $1500\times$, (c) $15,000\times$, and (d) $35,000\times$.

3.6. EIS Analysis of GCE and Cu₂O/GCE

The EIS analysis of GCE and Cu₂O/GCE was performed to evaluate the changes in the interfacial charge transfer resistance of the modified electrode. EIS in the form of a Nyquist plot features a semicircle in the higher frequency region corresponding to the electron-transfer-limited process and a straight line at the lower frequency region, which is due to a diffusion-limited process [53,54]. A Nyquist plot is typically used to distinguish between the successful modification, and the interpretation of the Nyquist plot relies on Randle's equivalent circuit model, where R_{ct} is the surface resistance of the modified electrode, C_{dl} is the capacitance of the electrical double layer, R_s is the solution resistance, and Z_w is the Warburg impedance of a diagonal line. The Nyquist plots of GCE and Cu₂O/GCE are presented in Figure 6a, where Cu₂O/GCE exhibited a distinctly larger semicircle compared to GCE, which is probably due to the presence of negatively charged functional groups at the modified electrode surface that hindered the electron transfer reaction between the Cu₂O/GCE and redox marker ($Fe(CN)_6^{3-/4-}$). The interactions, either attractive or repulsive, between the modified material at the surface of GCE and ($Fe(CN)_6^{3-/4-}$) were estimated on the basis of the comparison of the magnitude of the semicircular region in the impedance measurements. The attractive interactions are due to the surface positive charges, whereas the negative entities such as surface oxygen groups generate the repulsive influence under the applied biased conditions. The expanded semicircular region for the modified electrode compared to bare GCE is indicative of such interactions. When Cu₂O/GCE was investigated against ($Fe(CN)_6^{3-/4-}$), a distinctly larger semicircle was observed than for GCE, which is due to the repulsion between the oxygen functional groups at the modified surface and ($Fe(CN)_6^{3-/4-}$), thus elaborating the higher charge transfer activity or conductivity compared to the bare electrode [53,55]. Thus, the charge transfer activity of the GCE was greatly improved after being modified with Cu₂O. Moreover, this significant increase in charge transfer resistance successfully advocates the entire surface coverage of GCE by Cu₂O thin film. The increase in the Warburg impedance for the Cu₂O/GCE was also concurrent with the decrease in the diffusion rate.

3.7. CV Analysis of GCE and Cu₂O/GCE

Figure 6b represents the CV (black curve) obtained for GCE in 0.1 M pH 7 phosphate buffer with and without NH₃ (1 mM) casting on the electrode surface. The CV scans were initiated at all of the times at OCV to a vertex potential (E_1) +1.0 V. The cathodic sweep was recorded from +1.0 V to −1.0 V and the anodic sweep was recorded from −1.0 V to +1.0 V. There was no clear redox peak at GCE, which indicated that the oxidation or reduction reaction of NH₃ did not take place at GCE in the investigated potential window. Subsequently, the CV of Cu₂O/GCE was researched (without the presence of NH₃ on the surface, blue curve) in 0.1 M pH 7 phosphate buffer by starting at OCV until +1.0 V and sweeping from positive to negative potentials (reduction) with a scan rate of 100 mV/s followed by the anodic sweep (oxidation) in the reverse direction (Figure S2, Supplementary Information). As the aim of the present work is the formation and properties of Cu₂O thin film on GCE, only the potential range from +1.0 V to −1.0 V was scanned, which did not allow the formation of a passive layer. In the first anodic scan, from OCV until +1.0 V, the oxidation peak at ~+0.006 was due to the oxidation of Cu₂O into CuO. The cathodic scan of Cu₂O/GCE was characterized by a well-shaped reduction peak at ~−0.23 V, assigned to CuO conversion into Cu₂O [45,56–58]. It might be speculated that, at a sufficiently positive potential, all of the Cu₂O was converted to CuO, whereas it subsequently reduced to Cu₂O during the cathodic scan. The reduction of CuO was immediately followed by the reduction of Cu₂O into metallic copper (Cu) and, characteristically, the peak position of the second reduction was more negative as per literature interpretations [36,59]; however, in phosphate buffer medium, a second reduction peak was not observed. While, in the anodic scan, the oxidation of deposited Cu should produce two peaks; however, the oxidation of deposited Cu at the interface was not limited by diffusion, so most of the Cu appeared as Cu₂O at the interface and, upon reverting the potential sweep in the positive direction,

only one oxidation peak (~ -0.07) was observed due to Cu_2O converting into CuO in the form of a well-defined semi-reversible peak. Thus, affected by the electrolyte medium, the reduction peak was due to the electrode reductions of both CuO and Cu_2O and the oxidation peak was due to the oxidation of Cu_2O formed at the interface. Moreover, as the surface area of the oxidation peak was comparable to the reduction peak, it was supposed that all the Cu_2O was reversibly reduced into CuO . Thus, the CV results also supported the XRD and XPS interpretations of the presence of Cu_2O thin film on the surface of GCE. The appearance of only oxidation and reduction associated with Cu_2O might be useful in the electrocatalytic detection of NH_3 in the phosphate buffer electrolyte. Thus, thermally converted Cu_2O thin film enhanced the electrocatalytic activity of the GCE in a phosphate buffer medium.

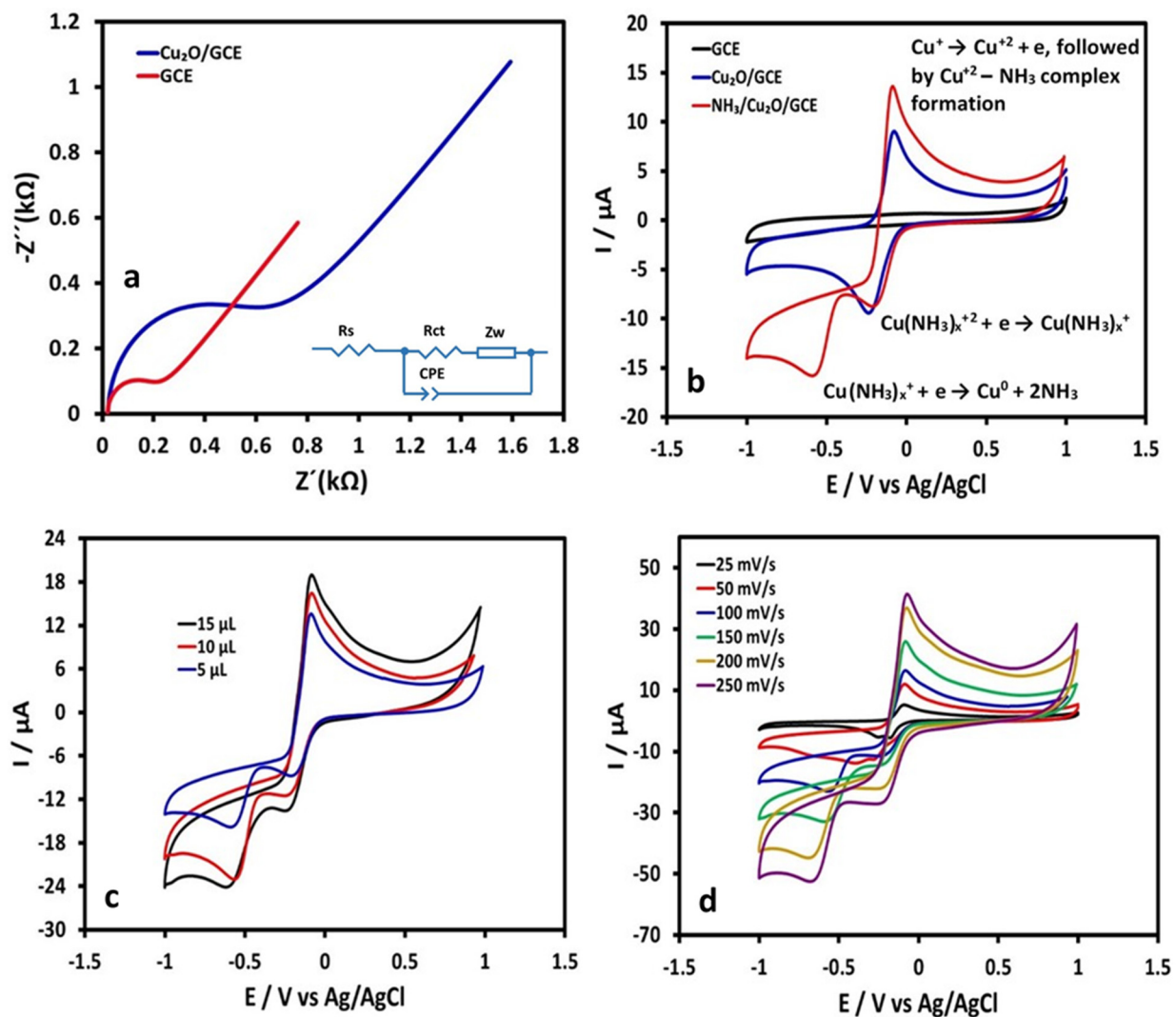
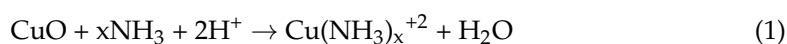


Figure 6. (a) Nyquist plot of GCE and $\text{Cu}_2\text{O}/\text{GCE}$, (b) CV curves of GCE, $\text{Cu}_2\text{O}/\text{GCE}$, and $\text{NH}_3/\text{Cu}_2\text{O}/\text{GCE}$ in 0.1 M pH 7 phosphate buffer, (c) $\text{Cu}_2\text{O}/\text{GCE}$ coating of different volumes and (d) effect of scan rate.

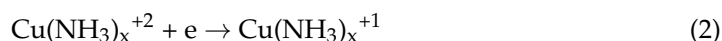
3.8. CV Analysis of $\text{NH}_3/\text{Cu}_2\text{O}/\text{GCE}$

The $\text{Cu}_2\text{O}/\text{GCE}$ was then covered with 10 μL of 1 mM NH_3 by drop coating and investigated in 0.1 M pH 7 phosphate buffer under the same CV conditions. The CV curve started from OCV and scanned between +1.0 V and -1.0 V is presented in Figure S2 (Supplementary Information). Under corresponding experimental conditions, however, in the presence of NH_3 over $\text{Cu}_2\text{O}/\text{GCE}$, the CV curve differed from the preceding. The presence of NH_3 on the modified electrode surface ensured the complex formation between

CuO and NH₃ when scanning reached +1.0 V [26,27]. This assumption is based on the possibility that NH₃ chemically reacts with CuO after it is formed [26,27,60]. The NH₃ covering favors the direct interaction between CuO and NH₃ and favors the electron transfer. However, an additional oxidation peak at +0.4 V (Figure S2, Supplementary Information) in the first anodic scan from OCV until +1.0 V may also be associated with the copper-ammonia complex formation. As was likely, it was found that by providing the same CV conditions, the NH₃/Cu₂O/GCE exhibited two reduction peaks in the cathodic scan and one oxidation peak in the reverse direction (Figure 6b, red curve). The anodic peak was more or less at the same potential value, however, the appearance of two reduction peaks at ~−0.57 and at ~−0.19, one small and one sharp, probably indicates the formation of a copper-ammonia complex. Different from the CV analysis of Cu₂O/GCE, the second reduction peak appeared at a more negative potential and was well separated from the first peak; therefore, it was chosen for the quantification of NH₃. The same has been reported elsewhere [26,27,60], in that the oxidation of Cu₂O in ammoniacal solution most likely went through the formation of the copper-ammonia complex and rather directly proceeded to form a passive layer, which subsequently reduced the electrocatalytic activity of the modified electrode. Since the NH₃/Cu₂O/GCE was exposed to the same experimental conditions as the Cu₂O/GCE, the consideration that the second reduction peak could arise due to the dissolution of the Cu₂O thin film was ruled out, but was due to the dissolution of NH₃. As a result, in the presence of NH₃, the anodic peak formed at ~−0.07 represented the oxidation of Cu₂O into CuO and the subsequent copper-ammonia complex formation according to the following equation,



In the reverse scan, the produced copper-ammine complex underwent two reductions according to the following reactions,



The first reaction was due to the reduction of the Cu(II)-ammonia complex into the Cu(I)-ammonia complex, whereas the second reaction represented the subsequent reduction of the Cu(I)-ammonia complex into Cu in a phosphate buffer medium. It can be further explained that, in the more positive potential, the reacting copper-ammine species were formed by complexation, and when the reverse bias was employed, the copper-ammine species depleted by two successive reductions into Cu. The second cathodic peak appeared due to the reaction of NH₃ with the Cu₂O thin film; thus, by examining the various CV effects on the second cathodic peak, the electrochemical detection of NH₃ was viable. Additionally, as the copper-ammonia complex formed at the modified electrode surface in a tiny amount, therefore, the exact coordination number of ammonia was uncertain.

3.9. Effect of Cu₂O Amount

The thickness of Cu₂O thin film is an important parameter to quantify the NH₃ [53]. The CVs of 1 mM NH₃ with three different thicknesses of Cu₂O thin film on GCE are presented in Figure 6c. As can be seen, by increasing the film thickness, the oxidation and reduction peak currents were also increased; however, the second reduction peak was eventually more affected. An insignificant change in the redox peaks associated with Cu₂O indicated these peaks were insensitive toward the presence of NH₃. Considering the second cathodic peak, at first, the current drastically increased from 5 μL to 10 μL and then approximately remained at the same intensity with a further increase in the film thickness. This phenomenon was caused by the presence of NH₃ on the surface of Cu₂O/GCE and indicated that the complex formation between CuO and NH₃ was adsorption-controlled due to the high concentration of Cu₂O. However, the further increase in the intensity of

the second cathodic peak with an increase in the Cu₂O film thickness was not observed because of the saturation. Thus, the changes in the second reduction peak current, caused by copper-ammonia complex reduction, were distinguishable due to different amounts of Cu₂O on GCE. Based on the above results, a 10- μ L coating of CuNPs was chosen as the optimal value.

3.10. Effect of the Scan Rate

The effects of the scanning rate on the reduction of the copper-ammonia complex were studied. The NH₃/Cu₂O/GCE was prepared by first depositing 10 μ L of CuNPs followed by thermal treatment, and then 10 μ L of 1 mM NH₃. Since the second cathodic peak originated from the complex formation between CuO and NH₃, this peak can be directly related to the presence of NH₃. The current of the second cathodic peak increased with the increase in the scan rate and was accompanied by a slight shift (Figure 6d) in the peak potential to the more negative direction due to the irreversible nature of the copper-ammonia reduction process. The peak current versus the scan rate is shown in Figure 7a, where a straight line with a correlation coefficient of 0.9941 also indicates the formation and reduction of the copper-ammonia complex were controlled by the adsorption process [34,49]. In Figure 7b, a plot of the logarithm of the peak current versus the logarithm of the scan rate is shown. The relationship was found to be linear with a slope of 0.97, which is far from the theoretical value of 0.5, suggesting that the detection of NH₃ is an adsorption-controlled rather than a diffusion-controlled process.

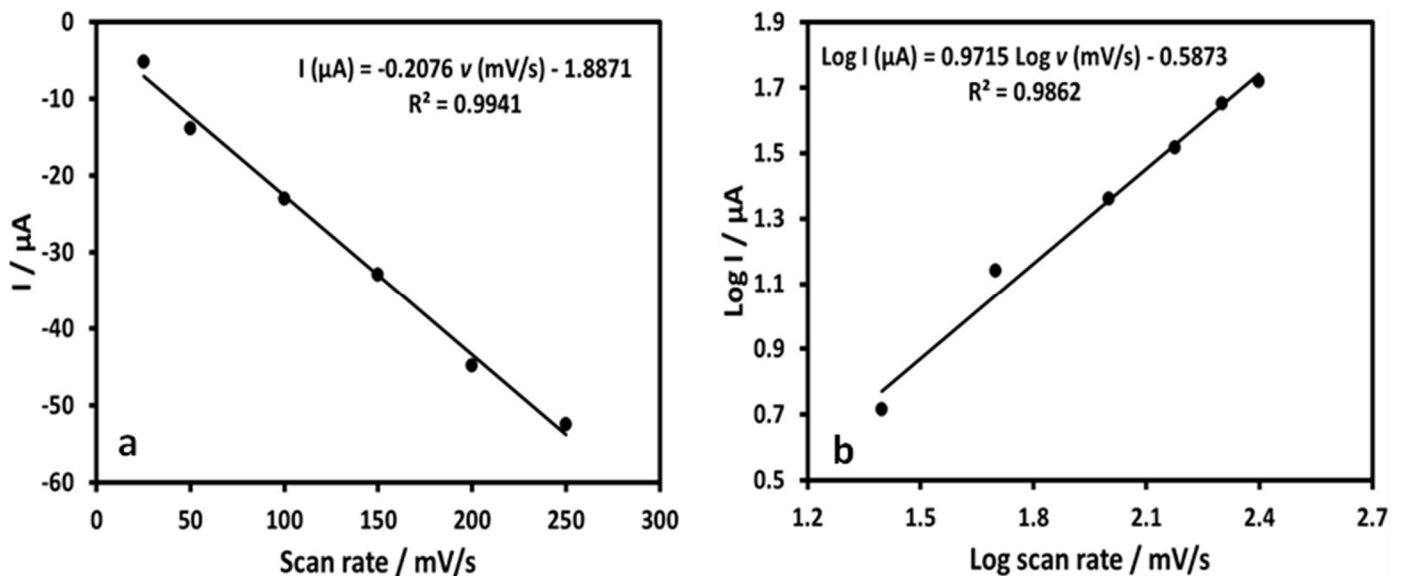


Figure 7. Plot of (a) the peak current versus the scan rate and (b) the logarithm of the peak current versus the logarithm of the scan rate.

3.11. Effect of NH₃ Concentration

Figure 8a shows the CVs of Cu₂O/GCE with different concentrations of NH₃ coated on it. The CVs were recorded under the same experimental conditions in 0.1 M pH 7 phosphate buffer and the concentrations of NH₃ were 0.01, 0.05, 0.1, 0.25, 0.5, 1, 2.5, and 5 mM, respectively. The current of the second cathodic peak significantly increased with the increasing concentration of NH₃. In Figure 8b, the reduction peak current as a function of the concentration of NH₃ is plotted. It was observed that the reduction peak current rapidly increased at low concentrations, followed by a gradual increase at high concentrations. This phenomenon is also attributable to the adsorption of NH₃ on the surface of Cu₂O/GCE [54].

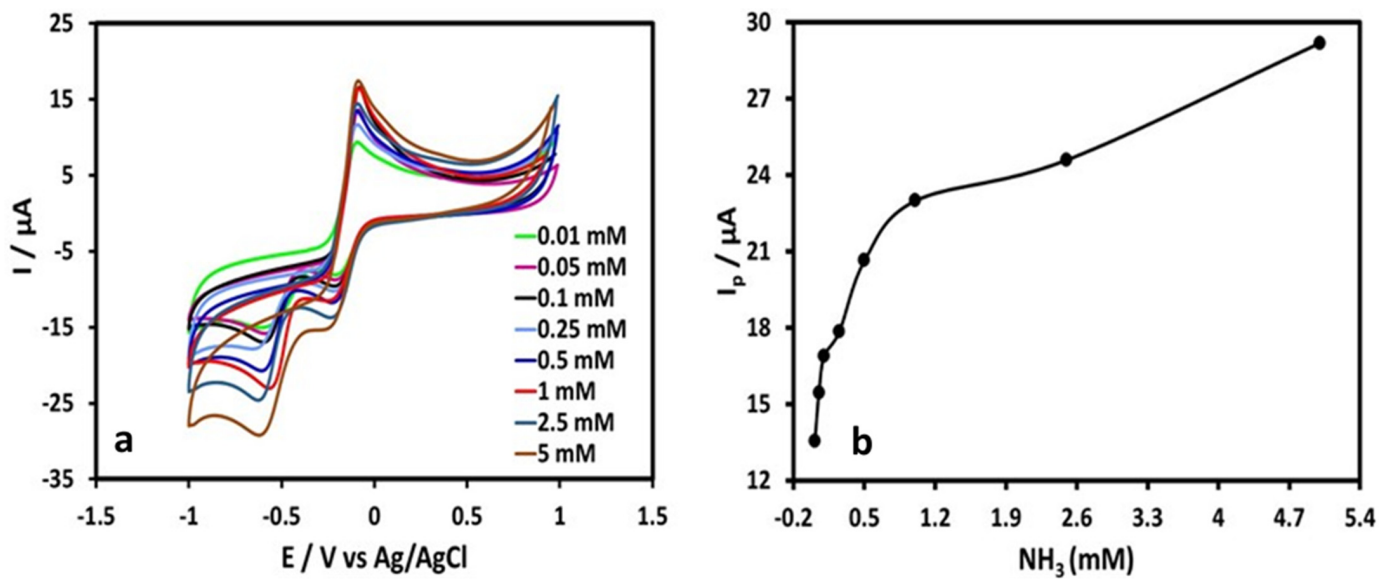


Figure 8. (a) CV curves of Cu₂O/GCE with different concentrations of NH₃ and (b) plot of peak current versus concentration of NH₃.

3.12. Effect of Changing the Vertex Potential

Further insights regarding the reduction of the copper-ammonia complex were extracted by inspecting the role of the vertex potential [36,59]. Figure 9a elaborates on the CV fetched by starting at OCV and sweeping between +0.2 V and -1.0 V. As discussed above, at a sufficiently positive potential, the majority of Cu₂O was oxidized into CuO, thus providing less positive E₁ potential. However, the appearance of two reduction peaks suggested that the copper-ammonia complex was successfully formed at such potential bias. The oxidation peak, which was due to the oxidation of interfacial Cu₂O, was slightly shifted toward a more positive potential and the associated cathodic peak appeared depressed, whereas the second cathodic peak was broad and higher in intensity, as compared to Figure 6c. Thus, a vertex potential less positive than +1.0 V also consisted of two reduction peaks and one oxidation peak, which suggested the utilization of a positive potential of less than +1.0 V may also be exploited in the detection of NH₃ over the Cu₂O/GCE.

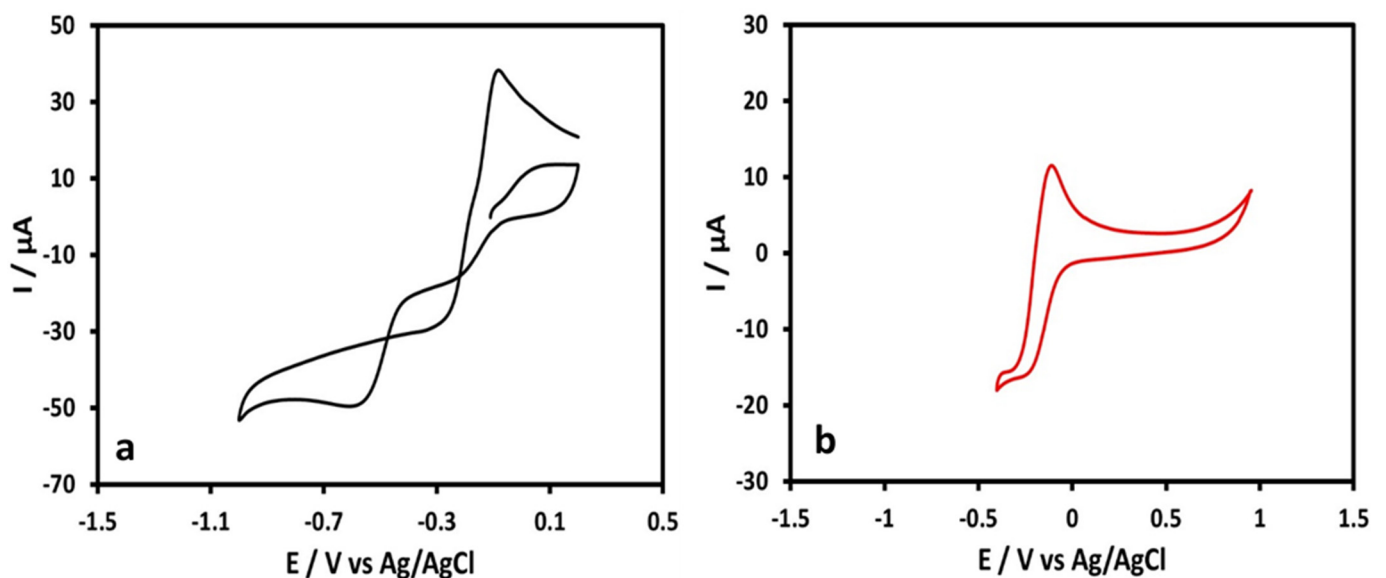


Figure 9. CV curves of NH₃/Cu₂O/GCE were obtained within the potential window of (a) +0.2 V and -1.0 V and (b) -0.4 V and +1.0 V.

In another potential bias (Figure 9b), from -0.4 V to $+1.0$ V, there was an oxidation peak that appeared due to the oxidation of Cu_2O to CuO , and an associated reduction peak was observed. In Figure S3 (Supplementary Information), the CV initiated at OCV with the first vertex potential was the same as in Figure 6b; however, the negative vertex potential was fixed at -0.4 V. The depressed reduction peak was due to the reduction of CuO into Cu_2O and, at a potential more negative than this, the deposition of Cu was possible. This means that, while reversing the scan from -0.4 V, there should be no oxidation peak, as the deposition of Cu was not undertaken. However, the appearance of a sharp and well-shaped oxidation peak established our assumption that the oxidation peak was due to the conversion of interfacial Cu_2O into CuO and not due to Cu deposited at the electrode surface limited by adsorption. These observations illustrate the importance of the changing vertex potentials that may notably affect the detection procedure.

3.13. Effect of the Supporting Electrolyte

The detection of NH_3 using the $\text{Cu}_2\text{O}/\text{GCE}$ in two more neutral pH-supporting electrolyte solutions, such as 0.1 M KCl and 0.1 M Na_2SO_4 , was tested. In both of the supporting electrolyte solutions, the CV with 10 μL of 1 mM NH_3 -coated $\text{Cu}_2\text{O}/\text{GCE}$ exhibited distinctly strong oxidation behavior, but no single reduction peak was witnessed (Figure 10a). The significant increase in the intensity of the oxidation peak current suggested that the electrodeposition of Cu during the cathodic sweep was significant as a result of a huge oxidation peak due to the anodic stripping of Cu observed in both KCl and Na_2SO_4 . No reduction peak was observed; thus, one thing was apparent, the copper-ammonia complex did not take place in these supporting electrolyte solutions, therefore, the pH 7 phosphate buffer was the ideal choice for the detection of NH_3 .

3.14. Effect of pH

The pH study of $\text{NH}_3/\text{Cu}_2\text{O}/\text{GCE}$ was carried out in the range of 4–10, and the obtained CVs are shown in Figure 10b. Due to the deposition of Cu at pH 4 and 5 during the cathodic sweep, the formed thin film was not stable, and resulted in a huge oxidation peak, as reported in the literature [26,45]. In other words, the copper-ammonia complex formation may take place in a neutral or basic medium. As can be seen, from within the pH range 6–10, under optimal conditions, the $\text{NH}_3/\text{Cu}_2\text{O}/\text{GCE}$ resulted in typical CV curves with three distinct redox peaks. The peak current versus pH plot in Figure 10c showed a gradual increase in the reduction current of the second cathodic peak from 6 to 7, while at pH 8 and 9, the current remained stable and then increased again at pH 10. These findings suggest the electrochemical detection of NH_3 at pH 7 or higher. So, for neutrality, pH 7 was preferred for further studies. Moreover, the peak potential versus pH plot (Figure 10d) displays a cathodic shift in the reduction peak potential of the second peak, which indicates the participation of protons in the reduction process of the copper-ammonia complex.

3.15. Effect of SWV Parameters

For the optimum detection of NH_3 in 0.1 M pH 7 phosphate buffer, the SWV response of the prepared $\text{NH}_3/\text{Cu}_2\text{O}/\text{GCE}$ was recorded. The SWV signal may be influenced by the variation in pulse amplitude, frequency, and step potential [53,54]. All three parameters are crucial for obtaining a sensitive SWV signal; therefore, the optimization of these parameters was performed, and the results are presented in Table 1. At first, the pulse amplitude was varied by keeping the other two parameters constant. The peak current increased with the increase in the pulse amplitude from 25 mV to 50 mV, followed by a gradual decrease. The maximum peak current observed at 50 mV was therefore chosen as the optimum value. The variation in the peak current with changing frequency reached the maximum at 50 ms; afterward, the peak shape was distorted and broad. The increase in the step potential resulted in a gradual increase in the peak current; however, the smooth and well-shaped SWV signal was observed at -10 mV. Thus, a 50 mV pulse amplitude, 50 ms frequency, and a -10 mV step potential were chosen as the optimum values for SWV investigations.

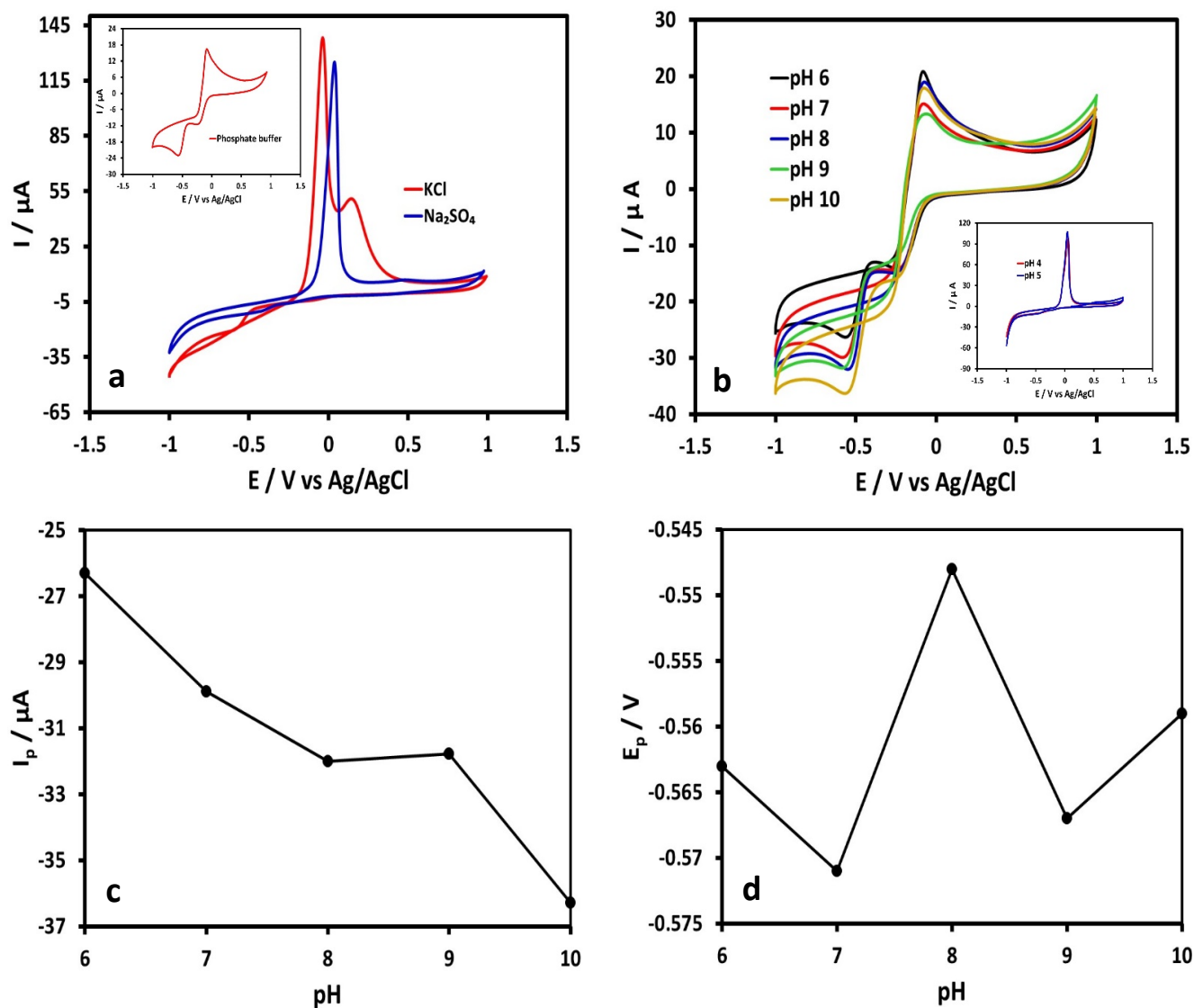


Figure 10. (a) CV curves of NH₃/Cu₂O/GCE in 0.1 M KCl and 0.1 M Na₂SO₄, (b) in different pH, (c) peak current versus pH plot, and (d) peak potential versus pH plot.

Table 1. SWV peak current and shape optimization.

Pulse Amplitude/mV	Frequency/ms	Step Potential/mV	I _p /μA
Pulse amplitude			
25	50	-10	-65.52
50	50	-10	-70.32
75	50	-10	-68.11
100	50	-10	-63.54
Frequency			
25	10	-10	-37.04
25	25	-10	-56.21
25	50	-10	-70.32
25	100	-10	-89.15
Step potential			
25	50	-5	-52.17
25	50	-10	-70.32
25	50	-15	-77.63
25	50	-20	-91.51

3.16. Analytical Response

The SWV analysis of $\text{NH}_3/\text{Cu}_2\text{O}/\text{GCE}$ showed a strong signal under optimum conditions. Figure 11a shows the SWVs of $\text{Cu}_2\text{O}/\text{GCE}$ with different NH_3 concentrations in the range of 10 μM to 1000 μM . Well-defined peaks proportional to the concentration of NH_3 were observed. The linear regression equation (Figure 11b) was $I_p (\mu\text{A}) = 50.497 C (\mu\text{M}) + 19.423$ ($R^2 = 0.9995$) with a detection limit ($3.3 \times$ standard deviation of blank/slope) of 6.23 μM determined at a single to noise ratio of 3, which was commensurate with the so far reported with a MWCNT/Cu nanocomposite paste electrode [17], considering the present work based on the NH_3 surface modification, and enabled the quick on-site testing of NH_3 in environmental samples. The sensor fabrication steps, as well as the detection medium, are important parameters to consider while developing an electrochemical sensor. As described in Table 2, though sensitive, most of the fabricated electrodes for NH_3 detection had complex structures that limited their widespread use and detected NH_3 through oxidation in very alkaline solutions. In comparison, the fabrication of $\text{NH}_3/\text{Cu}_2\text{O}/\text{GCE}$ was a two-step procedure and detection was unique in a neutral medium, which can easily be combined with disposable SPCE (screen-printed carbon paste electrode) for the portable detection of NH_3 .

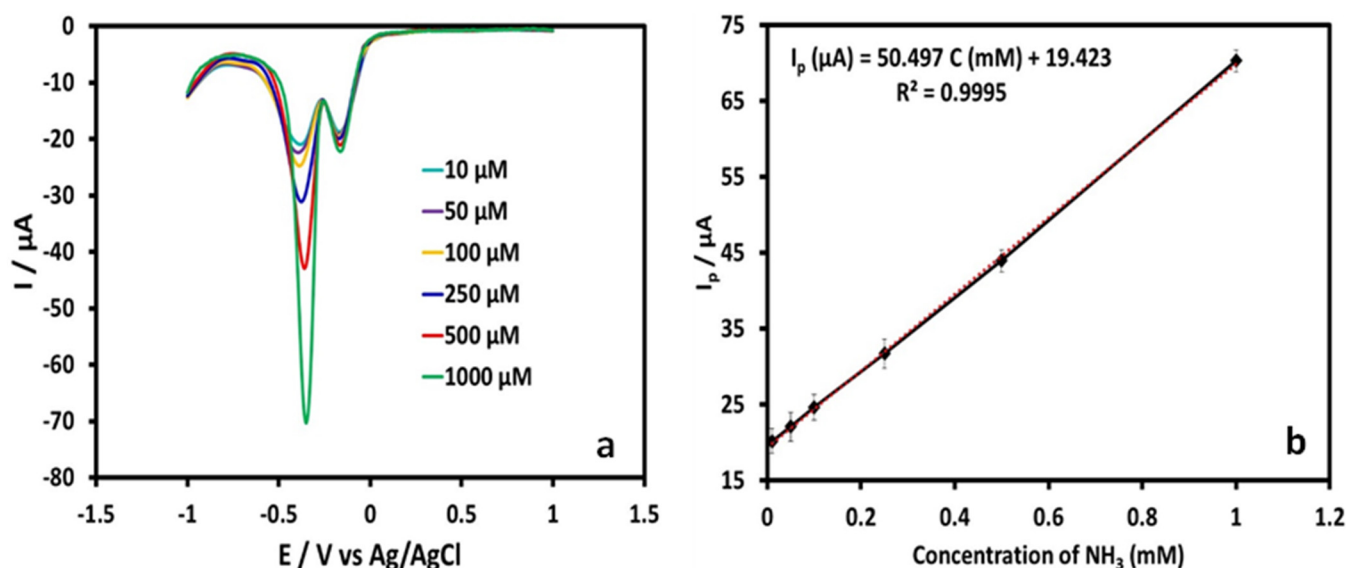


Figure 11. (a) SWV signal of $\text{Cu}_2\text{O}/\text{GCE}$ with NH_3 in the concentration range of 10 μM to 1000 μM and (b) peak current versus concentration of NH_3 plot.

Table 2. Comparison of various fabrication and detection procedures for detecting NH_3 .

Electrode System	Direct/Indirect Detection	Detection Technique	Supporting Electrolyte	Linear Range	LOD	References
$\text{NH}_3/\text{Cu}_2\text{O}$ NPs/GCE	Through complex formation/indirect	SWV	0.1 M Phosphate buffer, pH 7	0.01–1 mM	6.23 μM	This work
MWCNT/Cu paste electrode	Through complex formation/indirect	DPV	50 mM Carbonate buffer, pH 10	3–100 μM	3.47 μM	[17]
Pt-working-microfabricated electrode	Oxidation/direct	CV	Ionic liquid	1–20 ppm	1 ppm	[12]
GCE	Through chemical reaction/oxidation/indirect	SWV	0.1 M Borate buffer, pH 9	0–60 μM	0.71 μM	[7]
Pt/ITO	Oxidation/direct	LSW	0.5 M KOH	0.27–5 μM	3.946 μM	[61]
Pt-PANI-CC	Oxidation/direct	DPV	1 M KOH	0.5–550 μM	77.2 nM	[62]
SnO_2	Oxidation/direct	CV	Phosphate buffer	-	-	[3]

The repeatability variation coefficients calculated as relative standard deviations (RSD) at two concentrations, such as 50 μM and 500 μM , were 3.1% and 2.6%, displaying a good repeatability of the modified electrode. The reproducibility variation coefficients, also

estimated at these concentrations using three separately fabricated $\text{NH}_3/\text{Cu}_2\text{O}/\text{GCE}$, were 2.1% and 2.9%, respectively, demonstrating excellent fabrication reproducibility. Also, the influence of interfering species was investigated. The Cu_2O thin film structure stability was investigated by performing two successive CV scans of the same modification. The results are provided in Figure S4, Supplementary Information. The successive scans showed the same characteristic peaks, two reductions, and one oxidation. The oxidation and first reduction peaks were due to the $\text{Cu}_2\text{O}/\text{CuO}$ couple and were mainly unaffected. This also means that the Cu_2O thin film structure was still intact, however, the second reduction peak was drastically depressed and decreased in intensity because most of the NH_3 was removed from the modified surface by dissolution and went into the solution, and because the copper-ammonia complex reduction is limited by the adsorption, the decrease in peak intensity was rational. Therefore, it was preferred to freshly prepare $\text{NH}_3/\text{Cu}_2\text{O}/\text{GCE}$ for each measurement because the detection of NH_3 relied on the first cathodic scan. The ions used were K^+ , Na^+ , Zn^{2+} , Ca^{2+} , Cu^{2+} , SO_4^{2-} , Cl^- , NO_2^- , and NO_3^- . Virtually no interfering effects were observed for anions. The reason for this was due to the negatively functionalized surface of $\text{NH}_3/\text{Cu}_2\text{O}/\text{GCE}$, which repelled the anions. However, Zn^{2+} and Cu^{2+} faintly influenced the SWV single due to its affinity toward NH_3 .

3.17. NH_3 Recovery

The recovery of NH_3 was demonstrated in the drinking water sample. The pH of the real sample solution was maintained at pH 7. First, no second cathodic peak was observed when $\text{Cu}_2\text{O}/\text{GCE}$ was immersed in the real sample solution and the SWV signal was acquired under the optimized conditions. Subsequently, an amount of stock NH_3 solution was drop-coated on the $\text{Cu}_2\text{O}/\text{GCE}$ surface, and recovery of the added NH_3 was observed to be good for three determinations. The results are summarized in Table 3 and imply that the fabricated $\text{NH}_3/\text{Cu}_2\text{O}/\text{GCE}$ was capable of NH_3 determination in real drinking water samples.

Table 3. Determination of NH_3 in drinking water samples using the proposed method.

Detected (mM)	Added (mM)	Measured (mM)	Recovery (%)
0	0.01	0.00982	98.2 ± 4.59
0	0.05	0.04838	96.7 ± 4.87
0	0.1	0.0991	99.1 ± 4.13

Recovery is expressed as average \pm relative standard deviation ($n = 3$).

4. Conclusions

The simple, intelligent, fast, and portable electrochemical detection of NH_3 by drop coating on $\text{Cu}_2\text{O}/\text{GCE}$ was successfully demonstrated in a neutral medium. The detection was based on the chemical complexation between CuO and NH_3 at the modified electrode surface and its subsequent reduction in the reverse direction. The fabrication of $\text{Cu}_2\text{O}/\text{GCE}$ followed by NH_3 covering was also very simple. The approach is more promising and reliable than the usual detection of NH_3 and could benefit the on-site detection of NH_3 by utilizing disposable carbon electrodes and portable electrochemical instruments.

Supplementary Materials: The following supporting information can be downloaded at: <https://www.mdpi.com/article/10.3390/surfaces6040029/s1>, Figure S1. SEM image of bare GCE; Figure S2. CV curves of $\text{Cu}_2\text{O}/\text{GCE}$ and $\text{NH}_3/\text{Cu}_2\text{O}/\text{GCE}$ initiated at open circuit voltage to a vertex potential +1.0 V and end at +1.0 V; Figure S3. CV curves of $\text{NH}_3/\text{Cu}_2\text{O}/\text{GCE}$ initiated at open circuit voltage to a vertex potential +1.0 V and end at +1.0 V. The second vertex potential was -0.4 V; Figure S4. Two successive CV curves of $\text{NH}_3/\text{Cu}_2\text{O}/\text{GCE}$ initiated at open circuit voltage to a vertex potential +1.0 V and end at +1.0 V.

Author Contributions: S.A.K.: Conceptualization, Project Administration, Funding Acquisition. A.N.K.: Investigation, Conceptualization, Methodology, Supervision, Writing—original draft, Writing—review and editing. B.A.-J.: Investigation, Methodology, Software, Writing—original draft. L.A.T.: In-

vestigation, Software. M.A.: Methodology, Software, Investigation. W.A.B.: Funding Acquisition, Methodology. A.H.: Methodology, Writing—review and editing. M.T.S.: Conceptualization, Project Administration, Investigation, Methodology, Supervision, Writing—original draft, Writing—review and editing. All authors have read and agreed to the published version of the manuscript.

Funding: This project was funded by the Deanship of Scientific Research (DSR) at King Abdulaziz University, Jeddah, under grant no. (G-652-247-38). The authors, therefore, acknowledge with thanks DSR for technical and financial support.

Data Availability Statement: Data will be made available on request.

Acknowledgments: The authors would like to acknowledge the Department of Chemistry and Center of Excellence in Environmental Studies, King Abdulaziz University, and Ministry of Higher Education, Kingdom of Saudi Arabia, for providing the facilities to carry out this research work.

Conflicts of Interest: The authors declare that they have no known competing financial interests or personal relationships that could have appeared to influence the work reported in this paper.

References

1. Buzzeo, M.C.; Giovannelli, D.; Lawrence, N.S.; Hardacre, C.; Seddon, K.R.; Compton, R.G. Elucidation of the Electrochemical Oxidation Pathway of Ammonia in Dimethylformamide and the Room Temperature Ionic Liquid, 1-Ethyl-3-methylimidazolium bis (trifluoromethylsulfonyl) imide. *Electroanal. Int. J. Devoted Fundam. Pract. Asp. Electroanal.* **2004**, *16*, 888–896. [\[CrossRef\]](#)
2. Bhogadia, M.; Edgar, M.; Hunwin, K.; Page, G.; Grootveld, M. Detection and Quantification of Ammonia as the Ammonium Cation in Human Saliva by ¹H NMR: A Promising Probe for Health Status Monitoring, with Special Reference to Cancer. *Metabolites* **2023**, *13*, 792. [\[CrossRef\]](#) [\[PubMed\]](#)
3. Arya, S.; Riyas, M.; Sharma, A.; Singh, B.; Prerna Bandhoria, P.; Khan, S.; Bharti, V. Electrochemical detection of ammonia solution using tin oxide nanoparticles synthesized via sol–gel route. *Appl. Phys. A* **2018**, *124*, 1–7. [\[CrossRef\]](#)
4. Zhao, Y.; Shi, R.; Bian, X.; Zhou, C.; Zhao, Y.; Zhang, S.; Wu, F.; Waterhouse, G.I.; Wu, L.Z.; Tung, C.H.; et al. Ammonia detection methods in photocatalytic and electrocatalytic experiments: How to improve the reliability of NH₃ production rates? *Adv. Sci.* **2019**, *6*, 1802109. [\[CrossRef\]](#)
5. Siribunbandal, P.; Kim, Y.H.; Osotchan, T.; Zhu, Z.; Jaisutti, R. Quantitative colorimetric detection of dissolved ammonia using polydiacetylene sensors enabled by machine learning classifiers. *ACS Omega* **2002**, *7*, 18714–18721. [\[CrossRef\]](#) [\[PubMed\]](#)
6. Biswas, A.; Ghosh, B.; Dey, R.S. Refining the spectroscopic detection technique: A pivot in the electrochemical ammonia synthesis. *Langmuir* **2023**, *39*, 3810–3820. [\[CrossRef\]](#)
7. Panchompoo, J.; Compton, R.G. Electrochemical detection of ammonia in aqueous solution using fluorecamine: A comparison of fluorometric versus voltammetric analysis. *J. Electrochem.* **2012**, *18*, 437.
8. Khan, M.A.; Qazi, F.; Hussain, Z.; Idrees, M.U.; Soomro, S.; Soomro, S. Recent trends in electrochemical detection of NH₃, H₂S and NO_x gases. *Int. J. Electrochem. Sci.* **2017**, *12*, 1711–1733. [\[CrossRef\]](#)
9. Ji, X.; Banks, C.E.; Compton, R.G. The direct electrochemical oxidation of ammonia in propylene carbonate: A generic approach to amperometric gas sensors. *Electroanal. Int. J. Devoted Fundam. Pract. Asp. Electroanal.* **2006**, *18*, 449–455. [\[CrossRef\]](#)
10. Ji, X.; Compton, R.G. Determination of ammonia based on the electrochemical oxidation of N, N'-diphenyl-1, 4-phenylenediamine in propylene carbonate. *Anal. Sci.* **2007**, *23*, 1317–1320. [\[CrossRef\]](#)
11. Zolotov, S.A.; Vladimirova, E.V.; Dunaeva, A.A.; Shipulo, E.V.; Petrukhin, O.M.; Vatsuro, I.M.; Kovalev, V.V. Determination of the ammonium ion by voltammetry at the liquid-liquid interface using calixarenes as neutral carriers. *Russ. J. Electrochem.* **2014**, *50*, 940–946. [\[CrossRef\]](#)
12. Oudenhoven, J.F.M.; Knoben, W.; Van Schaijk, R. Electrochemical detection of ammonia using a thin ionic liquid film as the electrolyte. *Procedia Eng.* **2015**, *120*, 983–986. [\[CrossRef\]](#)
13. Vidal-Iglesias, F.J.; García-Aráez, N.; Montiel, V.; Feliu, J.M.; Aldaz, A. Selective electrocatalysis of ammonia oxidation on Pt (1 0 0) sites in alkaline medium. *Electrochem. Commun.* **2003**, *5*, 22–26. [\[CrossRef\]](#)
14. Bunce, N.J.; Bejan, D. Mechanism of electrochemical oxidation of ammonia. *Electrochim. Acta* **2011**, *56*, 8085–8093. [\[CrossRef\]](#)
15. Le Vot, S.; Roué, L.; Bélanger, D. Study of the electrochemical oxidation of ammonia on platinum in alkaline solution: Effect of electrodeposition potential on the activity of platinum. *J. Electroanal. Chem.* **2013**, *691*, 18–27. [\[CrossRef\]](#)
16. De Mishima, B.L.; Lescano, D.; Holgado, T.M.; Mishima, H.T. Electrochemical oxidation of ammonia in alkaline solutions: Its application to an amperometric sensor. *Electrochim. Acta* **1998**, *43*, 395–404. [\[CrossRef\]](#)
17. Valentini, F.; Biagiotti, V.; Lete, C.; Palleschi, G.; Wang, J. The electrochemical detection of ammonia in drinking water based on multi-walled carbon nanotube/copper nanoparticle composite paste electrodes. *Sens. Actuators B Chem.* **2007**, *128*, 326–333. [\[CrossRef\]](#)
18. Din, M.I.; Rehan, R. Synthesis, characterization, and applications of copper nanoparticles. *Anal. Lett.* **2017**, *50*, 50–62. [\[CrossRef\]](#)
19. Usman, M.S.; Ibrahim, N.A.; Shameli, K.; Zainuddin, N.; Yunus, W.M.Z.W. Copper nanoparticles mediated by chitosan: Synthesis and characterization via chemical methods. *Molecules* **2012**, *17*, 14928–14936. [\[CrossRef\]](#)

20. Ramyadevi, J.; Jeyasubramanian, K.; Marikani, A.; Rajakumar, G.; Rahuman, A.A. Synthesis and antimicrobial activity of copper nanoparticles. *Mater. Lett.* **2012**, *71*, 114–116. [[CrossRef](#)]
21. Gawande, M.B.; Goswami, A.; Felpin, F.X.; Asefa, T.; Huang, X.; Silva, R.; Zou, X.; Zboril, R.; Varma, R.S. Cu and Cu-based nanoparticles: Synthesis and applications in catalysis. *Chem. Rev.* **2016**, *116*, 3722–3811. [[CrossRef](#)] [[PubMed](#)]
22. Kodasi, B.; Joshi, S.D.; Kamble, R.R.; Keri, R.S.; Bayannavar, P.K.; Nesaragi, A.R.; Dixit, S.; Vootla, S.K.; Metre, T.V. Cu microcrystals garnished with copper nanoparticles catalyzed one-pot facile synthesis of novel 1, 2, 3-triazoles via click chemistry as antifungal agents. *Appl. Organomet. Chem.* **2022**, *36*, e6664. [[CrossRef](#)]
23. Kang, W.; Pei, X.; Bange, A.; Haynes, E.N.; Heineman, W.R.; Papautsky, I. Copper-based electrochemical sensor with palladium electrode for cathodic stripping voltammetry of manganese. *Anal. Chem.* **2014**, *86*, 12070–12077. [[CrossRef](#)] [[PubMed](#)]
24. Lete, C.; Spinciu, A.M.; Alexandru, M.G.; Calderon Moreno, J.; Leau, S.A.; Marin, M.; Visinescu, D. Copper (II) oxide nanoparticles embedded within a PEDOT matrix for hydrogen peroxide electrochemical sensing. *Sensors* **2022**, *22*, 8252. [[CrossRef](#)] [[PubMed](#)]
25. Bonthula, S.; Bonthula, S.R.; Pothu, R.; Srivastava, R.K.; Boddula, R.; Radwan, A.B.; Al-Qahtani, N. Recent Advances in Copper-Based Materials for Sustainable Environmental Applications. *Sustain. Chem.* **2023**, *4*, 246–271. [[CrossRef](#)]
26. Grujicic, D.; Pesic, B. Reaction and nucleation mechanisms of copper electrodeposition from ammoniacal solutions on vitreous carbon. *Electrochim. Acta* **2005**, *50*, 4426–4443. [[CrossRef](#)]
27. Zhybak, M.T.; Vagin, M.Y.; Beni, V.; Liu, X.; Dempsey, E.; Turner, A.P.; Korpan, Y.I. Direct detection of ammonium ion by means of oxygen electrocatalysis at a copper-polyaniline composite on a screen-printed electrode. *Microchim. Acta* **2016**, *183*, 1981–1987. [[CrossRef](#)]
28. Xiong, J.; Wang, Y.; Xue, Q.; Wu, X. Synthesis of highly stable dispersions of nanosized copper particles using L-ascorbic acid. *Green Chem.* **2016**, *13*, 900–904. [[CrossRef](#)]
29. Khan, A.; Rashid, A.; Younas, R.; Chong, R. A chemical reduction approach to the synthesis of copper nanoparticles. *Int. Nano Lett.* **2016**, *6*, 21–26. [[CrossRef](#)]
30. Chandra, S.; Kumar, A.; Tomar, P.K. Synthesis and characterization of copper nanoparticles by reducing agent. *J. Saudi Chem. Soc.* **2014**, *18*, 149–153. [[CrossRef](#)]
31. Shikha, J.A.I.N.; Ankita, J.A.I.N.; Kachhawah, P.; Devra, V. Synthesis and size control of copper nanoparticles and their catalytic application. *Trans. Nonferrous Met. Soc. China* **2015**, *25*, 3995–4000.
32. Ali Soomro, R.; Tufail Hussain Sherazi, S.; Memon, N.; Raza Shah, M.; Hussain Kalwar, N.; Richard Hallam, K.; Shah, A. Synthesis of air stable copper nanoparticles and their use in catalysis. *Adv. Mater. Lett.* **2014**, *5*, 191–198. [[CrossRef](#)]
33. Sood, A.; Arora, V.; Shah, J.; Kotnala, R.K.; Jain, T.K. Ascorbic acid-mediated synthesis and characterisation of iron oxide/gold core-shell nanoparticles. *J. Exp. Nanosci.* **2016**, *11*, 370–382. [[CrossRef](#)]
34. Bashami, R.M.; Soomro, M.T.; Khan, A.N.; Aazam, E.S.; Ismail, I.M.; El-Shahawi, M.S. A highly conductive thin film composite based on silver nanoparticles and malic acid for selective electrochemical sensing of trichloroacetic acid. *Anal. Chim. Acta* **2018**, *1036*, 33–48. [[CrossRef](#)] [[PubMed](#)]
35. Palomba, M.; Carotenuto, G.; Longo, A. A Brief Review: The Use of L-Ascorbic Acid as a Green Reducing Agent of Graphene Oxide. *Materials* **2022**, *15*, 6456. [[CrossRef](#)] [[PubMed](#)]
36. Stojanov, L.; Rafailovska, A.; Jovanovski, V.; Mirceski, V. Electrochemistry of Copper in Polyacrylic Acid: The Electrode Mechanism and Analytical Application for Gaseous Hydrogen Peroxide Detection. *J. Phys. Chem. C* **2022**, *126*, 18313–18322. [[CrossRef](#)]
37. Yabuki, A.; Tanaka, S. Oxidation behavior of copper nanoparticles at low temperature. *Mater. Res. Bull.* **2011**, *46*, 2323–2327. [[CrossRef](#)]
38. Yoon, J.; Choi, D.J.; Kim, Y.H. Fabrication of CuO and Cu₂O nanoparticles in a thick polyimide film by post heat treatment in a controlled-atmosphere. *J. Nanosci. Nanotechnol.* **2011**, *11*, 796–800. [[CrossRef](#)]
39. Umer, A.; Naveed, S.; Ramzan, N.; Rafique, M.S.; Imran, M. A green method for the synthesis of copper nanoparticles using L-ascorbic acid. *Matéria* **2014**, *19*, 197–203. [[CrossRef](#)]
40. Nguyen, V.T.; Trinh, K.S. In situ deposition of copper nanoparticles on polyethylene terephthalate filters and antibacterial testing against Escherichia coli and Salmonella enterica. *Braz. J. Chem. Eng.* **2020**, *36*, 1553–1560. [[CrossRef](#)]
41. Kim, Y.; Kim, M.G. HPLC-UV method for the simultaneous determinations of ascorbic acid and dehydroascorbic acid in human plasma. *Transl. Clin. Pharmacol.* **2016**, *24*, 37–42. [[CrossRef](#)]
42. Qi, F.; Huang, H.; Wang, M.; Rong, W.; Wang, J. Applications of antioxidants in dental procedures. *Antioxidants* **2022**, *11*, 2492. [[CrossRef](#)] [[PubMed](#)]
43. Koliou, E.K.; Ioannou, P.V. Preparation of dehydro-L-ascorbic acid dimer by air oxidation of L-ascorbic acid in the presence of catalytic amounts of copper (II) acetate and pyridine. *Carbohydr. Res.* **2005**, *340*, 315–318. [[CrossRef](#)] [[PubMed](#)]
44. Shafiey Dehaj, M.; Zamani Mohiabadi, M. Experimental study of water-based CuO nanofluid flow in heat pipe solar collector. *J. Therm. Anal. Calorim.* **2019**, *137*, 2061–2072. [[CrossRef](#)]
45. Zhang, Z.; Wang, P. Highly stable copper oxide composite as an effective photocathode for water splitting via a facile electrochemical synthesis strategy. *J. Mater. Chem.* **2012**, *22*, 2456–2464. [[CrossRef](#)]
46. Sudha, V.; Murugadoss, G.; Thangamuthu, R. Structural and morphological tuning of Cu-based metal oxide nanoparticles by a facile chemical method and highly electrochemical sensing of sulphite. *Sci. Rep.* **2021**, *11*, 3413. [[CrossRef](#)]
47. Kader, D.A.; Rashid, S.O.; Omer, K.M. Green nanocomposite: Fabrication, characterization, and photocatalytic application of vitamin C adduct-conjugated ZnO nanoparticles. *RSC Adv.* **2023**, *13*, 9963–9977. [[CrossRef](#)]

48. Li, J.; Mei, Z.; Liu, L.; Liang, H.; Azarov, A.; Kuznetsov, A.; Liu, Y.; Ji, A.; Meng, Q.; Du, X. Probing defects in nitrogen-doped Cu₂O. *Sci. Rep.* **2014**, *4*, 7240. [[CrossRef](#)]
49. Zhao, W.; Fu, W.; Yang, H.; Tian, C.; Li, M.; Li, Y.; Zhang, L.; Sui, Y.; Zhou, X.; Chen, H.; et al. Electrodeposition of Cu₂O films and their photoelectrochemical properties. *CrystEngComm* **2011**, *13*, 2871–2877. [[CrossRef](#)]
50. Won, Y.H.; Stanciu, L.A. Cu₂O and Au/Cu₂O particles: Surface properties and applications in glucose sensing. *Sensors* **2012**, *12*, 13019–13033. [[CrossRef](#)]
51. Aziz, G.E.N.Ç. Hydrothermal Synthesis of Cuprous Oxide Nanoflowers and Characterization of Their Optical Properties. *Süleyman Demirel Üniv. Fen Bilim. Enst. Derg.* **2018**, *22*, 397–401.
52. Mowbray, R. Morphological Control of Copper and Cuprous Oxide Nanoparticles via Synthesis and Oxidation/Reduction Reactions. Ph.D. Thesis, University of Colorado at Boulder, Boulder, CO, USA, 2013.
53. Bashami, R.M.; Hameed, A.; Aslam, M.; Ismail, I.M.; Soomro, M.T. The suitability of ZnO film-coated glassy carbon electrode for the sensitive detection of 4-nitrophenol in aqueous medium. *Anal. Methods* **2015**, *7*, 1794–1801. [[CrossRef](#)]
54. Kosa, S.A.M.; Khan, A.N.; Ahmed, S.; Aslam, M.; Bawazir, W.A.; Hameed, A.; Soomro, M.T. Strategic Electrochemical Determination of Nitrate over Polyaniline/Multi-Walled Carbon Nanotubes-Gum Arabic Architecture. *Nanomaterials* **2022**, *12*, 3542. [[CrossRef](#)] [[PubMed](#)]
55. Islam, M.M.; Diawara, B.; Maurice, V.; Marcus, P. Bulk and surface properties of Cu₂O: A first-principles investigation. *J. Mol. Struct. THEOCHEM* **2009**, *903*, 41–48. [[CrossRef](#)]
56. Zhang, W.; Yin, J.; Min, F.; Jia, L.; Zhang, D.; Zhang, Q.; Xie, J. Cyclic voltammetry analysis of copper electrode performance in Na₂WO₄ solution and optical property of electrochemical synthesized CuWO₄ nanoparticles. *J. Alloys Compd.* **2017**, *690*, 221–227. [[CrossRef](#)]
57. Han, U.B.; Lee, J.S. Integration scheme of nanoscale resistive switching memory using bottom-up processes at room temperature for high-density memory applications. *Sci. Rep.* **2016**, *6*, 28966. [[CrossRef](#)]
58. Mohammadzadeh, S.; Zare, H.R.; Khoshro, H. Electrochemical study of Cu₂O/CuO composite coating produced by annealing and electrochemical methods. *J. Iran. Chem. Soc.* **2019**, *16*, 2719–2729. [[CrossRef](#)]
59. Ramos, A.; Miranda-Hernández, M.; González, I. Influence of chloride and nitrate anions on copper electrodeposition in ammonia media. *J. Electrochem. Soc.* **2001**, *148*, C315. [[CrossRef](#)]
60. Hench-Cabrera, A.E.; Quiroga-González, E. Direct electrochemical detection mechanism of ammonia in aqueous solution using Cu-decorated Si microelectrodes. *J. Electrochem. Sci. Eng.* **2023**. [[CrossRef](#)]
61. Wang, J.; Diao, P. Simultaneous detection of ammonia and nitrate using a modified electrode with two regions. *Microchem. J.* **2020**, *154*, 104649. [[CrossRef](#)]
62. Zhang, L.; Liu, T.; Ren, R.; Zhang, J.; He, D.; Zhao, C.; Suo, H. In situ synthesis of hierarchical platinum nanosheets-polyaniline array on carbon cloth for electrochemical detection of ammonia. *J. Hazard. Mater.* **2020**, *392*, 122342. [[CrossRef](#)] [[PubMed](#)]

Disclaimer/Publisher's Note: The statements, opinions and data contained in all publications are solely those of the individual author(s) and contributor(s) and not of MDPI and/or the editor(s). MDPI and/or the editor(s) disclaim responsibility for any injury to people or property resulting from any ideas, methods, instructions or products referred to in the content.